Optimal Porosity Distribution for Minimized Ohmic Drop across a Porous Electrode

Venkatasailanathan Ramadesigan,[a,*] Ravi N. Methekar,[a,*] Folarin Latinwo,[b] Richard D. Braatz,[b,c] and Venkat R. Subramanian[a,**,z]

[a]*Department of Energy, Environmental and Chemical Engineering, Washington University, St. Louis, Missouri 63130, USA*
[b]*Chemical and Biomolecular Engineering, University of Illinois at Urbana-Champaign, Urbana, Illinois 61801, USA*
[c]*Department of Chemical Engineering, Massachusetts Institute of Technology, Cambridge, Massachusetts 02139, USA*

This paper considers the design of spatially varying porosity profiles in next-generation electrodes based on simultaneous optimization of a porous-electrode model. Model-based optimal design (not including the solid-phase intercalation mechanism) is applied to a porous positive electrode made of lithium cobalt oxide, which is commonly used in lithium-ion batteries for various applications. For a fixed amount of active material, optimal grading of the porosity across the electrode was found to decrease the ohmic resistance by 15%–33%, which in turn increases the electrode capacity to hold and deliver energy. The optimal porosity grading was predicted to have 40% lower variation in the ohmic resistance to variations in model parameters due to manufacturing imprecision or capacity fade. The results suggest that the potential for the simultaneous model-based design of electrode material properties that employ more detailed physics-based first-principles electrochemical engineering models to determine optimal design values for manufacture and experimental evaluation.
© 2010 The Electrochemical Society. [DOI: 10.1149/1.3495992] All rights reserved.

Electrochemical power sources have had significant improvements in design and operating range and are expected to play a vital role in the future in automobiles, power storage, military, and space applications. Lithium-ion chemistry has been identified as a preferred candidate for high-power/high-energy secondary batteries. Applications for batteries range from implantable cardiovascular defibrillators operating at 10 μA current to hybrid vehicles requiring pulses of up to 100 A. Today, the design of these systems have been primarily based on (i) matching the capacity of anode and cathode materials; (ii) trial-and-error investigation of thickness, porosity, active material, and additive loading; (iii) manufacturing convenience and cost; (iv) ideal expected thermal behavior at the system level to handle high currents; and (v) detailed microscopic models to understand, optimize, and design these systems by changing one or few parameters at a time.

Traditionally, macroscopic models have been used to optimize the electrode thickness or spatially uniform porosity in lithium-ion battery design. Many applications of mathematical modeling to design Li-ion batteries are available in the literature.[1-10] An approach to identify the optimal values of system parameters such as electrode thickness has been reported by Newman and co-workers.[2,5-10] Simplified models based on porous-electrode theory can provide analytical expressions to describe the discharge of rechargeable lithium-ion batteries in terms of the relevant system parameters. Newman and co-workers[2,5-8] have utilized continuum electrochemical engineering models for design and optimization as a tool for the identification of system limitations from the experimental data. Equations were developed that describe the time dependence of potential as a function of electrode porosity and thickness, the electrolyte and solid-phase conductivities, specific ampere-hour capacity, separator conductivity and thickness, and current density. Analysis of these equations yields the values of electrode porosity and electrode thickness so as to maximize the capacity for discharge to a given cutoff potential.[2] Simplified models based on porous-electrode theory were used to describe the discharge of rechargeable lithium batteries and derive analytical expressions for the cell potential, specific energy, and average power in terms of the relevant system parameters. The resulting theoretical expressions were used for design and optimization

purposes and for the identification of system limitations from experimental data.[5] Studies were performed by comparing the Ragone plots for a range of design parameters. A single curve in a Ragone plot involves hundreds of simulations wherein the applied current is varied over a wide range of magnitude. Ragone plots for different configurations are obtained by changing the design parameters (e.g., thickness) one at a time and by keeping the other parameters at constant values. This process of generating a Ragone plot is quite tedious, and typically Ragone curves reported in the literature are not smooth due to computational constraints. Batteries are typically designed only to optimize the performance at the very first cycle of operation of the battery, whereas in practice most of the battery's operation occurs under significantly degraded conditions. Further, multivariable optimization is not computationally efficient using most first-principles models described in the literature. A reformulated model[11,12] is sufficiently computationally efficient to enable the simultaneous optimal design of multiple parameters over any number of cycles by including the mechanisms for capacity fade. Further, this model can be used to quantify the effects of model uncertainties and variations in the design parameters on the battery performance. Recently, such an application was reported in which the utilization averaged over 1000 cycles was maximized for a battery design obtained by simultaneous optimization of the applied current density (I) and thickness of the separator and the two electrodes (l_s, l_n, l_p) for cycle 1, and the effects of variations in these four design parameters due to imprecise manufacturing were investigated.[13] The battery design optimized for cycle 1 did not maximize the cycle-averaged utilization.

This paper designs spatially varying porosity profiles in porous electrodes based on simultaneous optimization applied to a porous-electrode model. The next section describes the simple electrochemical porous-electrode model used in this study. Then different methods for the simultaneous optimization of model parameters are discussed. The optimization procedure used in this study is then described, followed by the results and discussion and conclusions.

Electrochemical Porous-Electrode Model

Garcia et al.[14] provided a framework for modeling microstructural effects in electrochemical devices. That model can be extended to treat more complex microstructures and physical phenomena such as particle distributions, multiple electrode phase mixtures, phase transitions, complex particle shapes, and anisotropic solid-state diffusivities. As mentioned earlier, there are several treatments for

* Electrochemical Society Student Member.
** Electrochemical Society Active Member.
z E-mail: vsubramanian@seas.wustl.edu

dealing with the microstructure of the porous electrodes in Li-ion batteries. However, there is no mention in the literature of using these models in optimization algorithms to extract optimal values of design parameters and hence perform model-based design for porous electrodes. As an initial investigation into the potential of such an approach, we employ a simple model for a porous electrode with parameters matched to that of a cathode of a Li-ion battery to verify the feasibility of simultaneous optimization of design parameters and to investigate whether employing more detailed models for optimization is worthwhile.

This paper considers the optimization of a single porous positive electrode where the electrode has the current collector at one end ($x = 0$) and electrolyte separator at the other end ($x = l_p$). The expressions for current in the solid phase (i_1) and electrolyte phase (i_2) are given by[1]

$$i_1 = -\sigma(x)\frac{d\Phi_1}{dx} \qquad [1]$$

$$i_2 = -\kappa(x)\frac{d\Phi_2}{dx} \qquad [2]$$

where σ is the electrical conductivity, κ is the ionic conductivity, and Φ_1 and Φ_2 are the solid-phase and electrolyte-phase potentials, respectively. The total applied current density across the cross-section of the electrode is equal to the sum of the solid-phase and liquid-phase current densities,

$$i_{app} = i_1 + i_2 \qquad [3]$$

The electrochemical reaction occurs at the solid–liquid interface with the solid-phase current (i_1), which is assumed to be related to the distance across the electrode (x) by linear kinetics,

$$\frac{di_1}{dx} = a(x)i_0\frac{F}{RT}(\Phi_1 - \Phi_2) \qquad [4]$$

with the active surface area given by

$$a(x) = \frac{3(1 - \varepsilon(x))}{R_p} \qquad [5]$$

R_p is the particle radius of active materials in the porous electrode, and $\varepsilon(x)$ is the spatially varying porosity in the electrode. The electrical and ionic conductivities are related to the spatially varying porosity by

$$\sigma(x) = \sigma_0(1 - \varepsilon(x))^{brugg} \qquad [6]$$

$$\kappa(x) = \kappa_0\varepsilon(x)^{brugg} \qquad [7]$$

where *brugg* is the Bruggeman coefficient to account for the tortuous path in the porous electrode. The boundary conditions for solution of these equations are

$$\Phi_1|_{x=0} = 1$$

$$\Phi_2|_{x=l_p} = 0$$

$$i_1|_{x=l_p} = 0 \qquad [8]$$

The ohmic resistance of this electrode is obtained by

$$\psi = \frac{\Phi_1|_{x=0} - \Phi_2|_{x=l_p}}{i_{app}} \qquad [9]$$

$$i_{app} = -\sigma(x)\left.\frac{d\Phi_1}{dx}\right|_{x=0} \qquad [10]$$

The above equations apply for any continuous or discontinuous functional form for $\varepsilon(x)$ and can be extended to more detailed microscale models for the conductivities and transport parameters as a function of porosity. Garcia et al.[14] considered detailed microstructure while modeling and identifying porosity or particle size varia-

tions in the electrodes to maximize performance. Previous efforts have considered atomistic simulations of batteries,[15] microstructural simulations,[16] and modeling the relationships between the properties and microstructure of the materials within packed multiphase electrodes. In this manuscript the robustness of its optimal design results to the use of a simple model in the optimization of the porous electrode is taken into account by analyzing the effects of variations in the model parameters.

The electrochemical modeling equations are usually solved by setting the applied current and computing the voltage, or vice versa. Many practical devices operate at constant-current or constant-power mode. It is important to realize that the capacity of each device is limited by the state variables and theoretical capacity of the material. To solve the mathematical model for a practical electrochemical device, it is necessary to obtain the physically realizable current value to be applied to or drawn from the electrode.

Constant-current method.— For solving this model for constant current, the constant current i_{app} would be set and the modeling equations simulated for the variables like Φ_1, Φ_2, and i_1 as given in Eq. 1-7. Equation 8 gives the boundary conditions for the constant-current method. Then the resistance (ψ) is computed using the output equation, Eq. 9. This procedure is easy to implement and the model equations are straightforward to simulate. However, the applied fixed current may not be commensurate with the capacity of the given battery and there is a chance of obtaining physically inconsistent results such as a predicted potential of -100 or $+1000$ V. To avoid this potential error, the constant-potential method has been used as described in next subsection.

Constant-potential method.— To avoid the shortcoming of the constant-current method, the constant-potential method was used in this study. In this method, the potential (Φ_1, Φ_2) is set and the current is treated as the output. This is done by solving i_{app} as the unknown variable in the model equations, Eq. 1-7. Then the resistance (ψ) is computed using the output equation, Eq. 9. The new boundary conditions are

$$\Phi_1|_{x=0} = 1$$

$$\Phi_2|_{x=l_p} = 0$$

$$i_1|_{x=l_p} = 0$$

$$i_{app} = -\sigma(x)\left.\frac{d\Phi_1}{dx}\right|_{x=0} \qquad [11]$$

This approach incorporates one additional boundary condition for describing the relationship of the applied current with the state variables. The advantage of this procedure is that the current has been determined using the state variables of the battery instead of being fixed to a preset number by the modeler. This computationally robust approach ensures that the voltage and current are at physically consistent values.

Optimization Procedure

A general formulation for the model-based optimal design of a system is[22]

$$\min_{\mathbf{z}(x),\mathbf{u}(x),\mathbf{p}} \Psi \qquad [12]$$

$$\text{such that } \frac{d}{dx}\mathbf{z} = \mathbf{f}(\mathbf{z}(x),\mathbf{y}(x),\mathbf{u}(x),\mathbf{p}), \quad \mathbf{f}(\mathbf{z}(0)) = 0, \quad \mathbf{g}(\mathbf{z}(1)) = 0$$
$$[13]$$

$$\mathbf{g}(\mathbf{z}(x),\mathbf{y}(x),\mathbf{u}(x),\mathbf{p}) = 0 \qquad [14]$$

$$\mathbf{u}_L \leq \mathbf{u}(x) \leq \mathbf{u}_U, \quad \mathbf{y}_L \leq \mathbf{y}(x) \leq \mathbf{y}_U, \quad \mathbf{z}_L \leq \mathbf{z}(x) \leq \mathbf{z}_U \quad [15]$$

where Ψ is the battery design objective to be minimized,[17] $\mathbf{z}(x)$ is the vector of differential state variables, $\mathbf{y}(x)$ is the vector of algebraic variables, $\mathbf{u}(x)$ is the vector of control variables, and $\mathbf{p}$ is the vector of design parameters. Different methods are available for solving constrained optimization problems, which include (i) variational calculus, (ii) Pontryagin's maximum principle, (iii) control vector iteration (CVI), (iv) control vector parameterization (CVP), and (v) simultaneous nonlinear programming.[18]

Complexities of optimization for battery models.— For a pseudo-two-dimensional battery model with 12 partial differential equations (PDEs), assume that the cathode, separator, and anode are discretized into 50 equally spaced node points in x and 20 nodes in r for each x. For the three regions (cathode, separator, and anode) the model will have 2400 differential algebraic equations (DAEs), which includes $50 \times 20 = 1000$ equations each for the cathode and anode for the solid phase, 50 differential equations for the electrolyte concentration, 50 algebraic equations for the electrolyte potential (potential in the electrolyte phase), and 50 algebraic equations for the solid-phase potential each for the cathode and anode. For the same number of node points in x, the separator has 50 differential equations for the electrolyte concentration and 50 algebraic equations for the electrolyte potential. In total, the number of DAEs to solve becomes $2 \times 1000 + 2 \times 150 + 100 = 2400$. Simultaneous optimization of many design valuables for a highly stiff system with 2400 DAEs is computationally expensive.

Indirect dynamic optimization methods such as variational calculus and Pontryagin's maximum principle method result in boundary value problems that are very difficult to solve for large systems of highly stiff nonlinear DAEs.[19] Direct methods for the solution of dynamic optimizations have gained prominence in the past few decades, in which the optimal solution is achieved by converting the optimization problem into nonlinear program using such methods as CVI, CVP, and simultaneous nonlinear programming.[20] Control vector parameterization is one of the commonly used methods and is the easiest method to implement. In the context of this particular application, the control variable $\mathbf{u}(x)$ is parameterized by a finite number of parameters, typically as a polynomial or piecewise-linear function or by partitioning its values over space, and the resulting nonlinear program is solved numerically. Most numerical optimization algorithms utilize an analytically or numerically determined gradient of the optimization objective and constraints to march toward improved values for the optimization variables in the search space. While advances in simultaneous discretization have been made in the field of global dynamic optimization,[21] today's algorithms are still too computationally expensive to be used in electrochemical processes, which are usually highly stiff with highly nonlinear kinetics and requires adaptive time-stepping, stiff solvers, etc. The simultaneous simulation-optimization approach,[18] which fixes the time or independent variable discretization a priori, is not computationally efficient for highly stiff DAEs such as arise in electrochemical processes. For example, for battery models with 2400 DAEs, the simultaneous simulation-optimization approach may result in millions of equations in the resulting nonlinear program. Based on our experience, battery models may not converge easily with direct discretization schemes in time.

In CVP, as the number of intervals increases, the number of equations increases tremendously and makes optimization computationally very expensive. Hence the fastest and most efficient model and code is recommended for CVP or any of the optimization methods. In this paper, as a first step, a simple model used that represents the essential dynamics of a porous electrode used in a lithium-ion battery. This model along with CVP makes the optimization computationally efficient and enables the implementation of additional runs to evaluate the global optimality of the computed design variables.

Optimization using CVP

In this paper, CVP is used to simultaneously optimize multiple parameters describing a spatial profile of porosity of an electrode in a lithium-ion battery. The numerical optimization was carried out using Marquardt's method,[22] in which new parameter values for the next iteration are related to the gradient multiplied by the old values of the design parameters. The numerical algorithm was repeated until a prespecified tolerance on the change in the design parameters was met.

In this formulation, the control variable (i.e., porosity) is partitioned across the electrode length. In each partition, the modeling equations, Eq. 1-11, are solved as a function of porosity. The boundary conditions at each partition are matched using the flux balance of the species. The number of equations is directly proportional to the number of partitions. The number of boundary conditions will also increase with the number of equations and partitions. The optimization objective was to minimize the ohmic resistance (ψ) across the electrode thickness in Eq. 1 for the control variable $u(x) = \varepsilon(x)$ subject to the constraints

(a) $0 < \varepsilon(x) < 1$,

(b) Average $\{\varepsilon_i\} < 0.4$, where $i = 1, \ldots, N$ (when a specific amount of active material is desired),

(c) Eq. 1-11, where $\mathbf{y}(i) = [\Phi_{(1,i)}, \Phi_{(2,i)}, i_{(1,i)}]$ and $0 \leq x \leq l_p$,

$$i_{(1,i)} = -\sigma_i \frac{\partial \Phi_{(1,i)}}{\partial x}$$

$$i_{(2,i)} = -\kappa_i \frac{\partial \Phi_{(2,i)}}{\partial x}$$

$$\frac{\partial i_{(1,i)}}{\partial x} = a_i i_0 \frac{F}{RT}(\Phi_{(1,i)} - \Phi_{(2,i)})$$

$$a_i = \frac{3(1 - \varepsilon_i)}{R_p}$$

(d) Boundary conditions for accommodating the partitions across the electrode are

$$\Phi_{(1,i)}|_{x=l_p/N} = \Phi_{(1,i+1)}|_{x=0}$$

$$\Phi_{(2,i)}|_{x=l_p/N} = \Phi_{(2,i+1)}|_{x=0}$$

$$i_{(1,i)}|_{x=l_p/N} = i_{(1,i+1)}|_{x=0}$$

where i indicates the ith partition and $x = 0$ and $x = l_p/N$ indicate the starting and ending spatial boundaries of the ith partition. The nonnegativity constraint is imposed on the porosity and the average-value constraint is imposed when a specific amount of active material is desired in the electrode. The ohmic resistance is calculated as a function of the porosity from the modeling equations. The model equations along with fixed boundary conditions and boundary conditions arising from CVP were solved using a boundary value problem (BVP) solver. Table I shows the base set of parameters used for the simulation of the model equations, Eq. 1-11, at various conditions. All simulations are performed using Maple® 13's BVP solver using a personal computer with a 3 GHz Intel® Core 2 Duo processor and 3.25 GB of RAM.

Results and Discussion

Optimization results of uniform porosity.— Figure 1 shows the variation in the total resistance across the porous electrode as a function of spatially uniform porosity obtained by brute-force gridding of the porosity, which shows a clearly identifiable optimal porosity of ~ 0.2. The same results for the $N = 1$ stage can be obtained using an analytical solution commonly used for porous electrodes

Table I. List of parameters used for the simulation (LiCoO$_2$ chemistry).

Parameter	Symbol	Parameter values
Electrical conductivity	σ_0	100 S/m
Bruggeman coefficient	*brugg*	1.5
Ionic conductivity	κ_0	20 S/m
Particle radius of the active materials	R_p	5.0×10^{-6} m
Length of the electrode	l_p	8×10^{-5} m
Faraday constant	F	96 487 C/mol
Ideal gas constant	R	8.314 J/(mol · K)
Temperature	T	298.15 K
Exchange current density	i_0	1×10^{-3} A/m^2

and as discussed in the Appendix. Operating with the porous electrode at this optimum porosity should provide the best performance for a system described by the model, Eq. 1-11. Figure 2a shows the convergence of the numerical optimization to the globally optimal value of the spatially uniform electrode porosity. This plot was constructed by optimizing the electrochemical model described in the section "Electrochemical porous-electrode model" starting at three different initial guesses (the third guess being the optimal value obtained in Fig. 1) for the electrode porosity. The final converged value for the electrode porosity was the same for many different initial guesses (two of which are shown in Fig. 2a). Figure 2b shows the convergence of the ohmic resistance across the electrode to the same single optimal value. A very low resistance was achieved by using the globally optimal value for the porosity of the electrode. Significant improvements in terms of performance were achieved by numerical optimization; the optimal design is about 15% more efficient in comparison with an average value of 0.4 used in practice for the electrode porosity for this chemistry.

Optimization results of graded porosity.— Numerical optimization was performed for a porous electrode with a graded porosity, that is, porosity that varies as a function of distance across the electrode. A recent patent (U.S. patent 7553584) proposed the use of graded porosity described by a functional form for betterment of the performance of the porous electrode. Functional forms of porosity may be implemented for theoretical studies but to practically fabri-
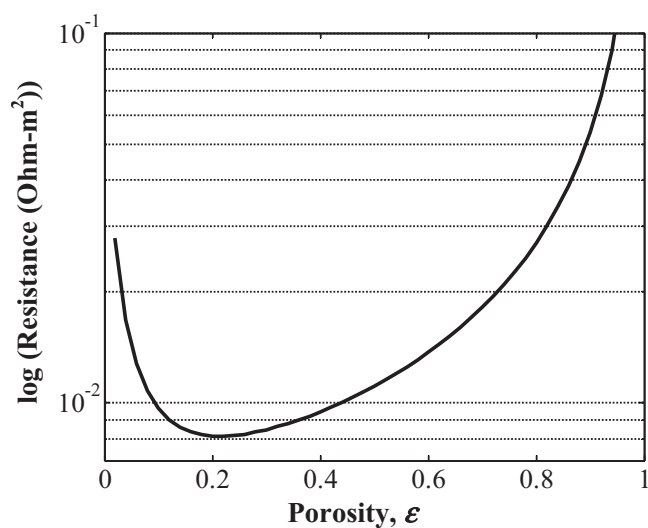

(a)

(b)

Figure 2. (a) Convergence to the optimal spatially uniform porosity ε starting from different initial guesses for the porosity; (b) corresponding convergence of the ohmic resistance.

Figure 1. Resistance vs porosity, ε. The plot was constructed by computing the resistance from the model equations Eq. 5-11 for each value of spatially uniform porosity between 0 and 1. Note that the unit of resistance reported here is Ohm-m^2 and can be converted to Ohm-m (typically reported in the literature), by dividing with the thickness of the electrode. The choice of the unit does not affect the optimization results.
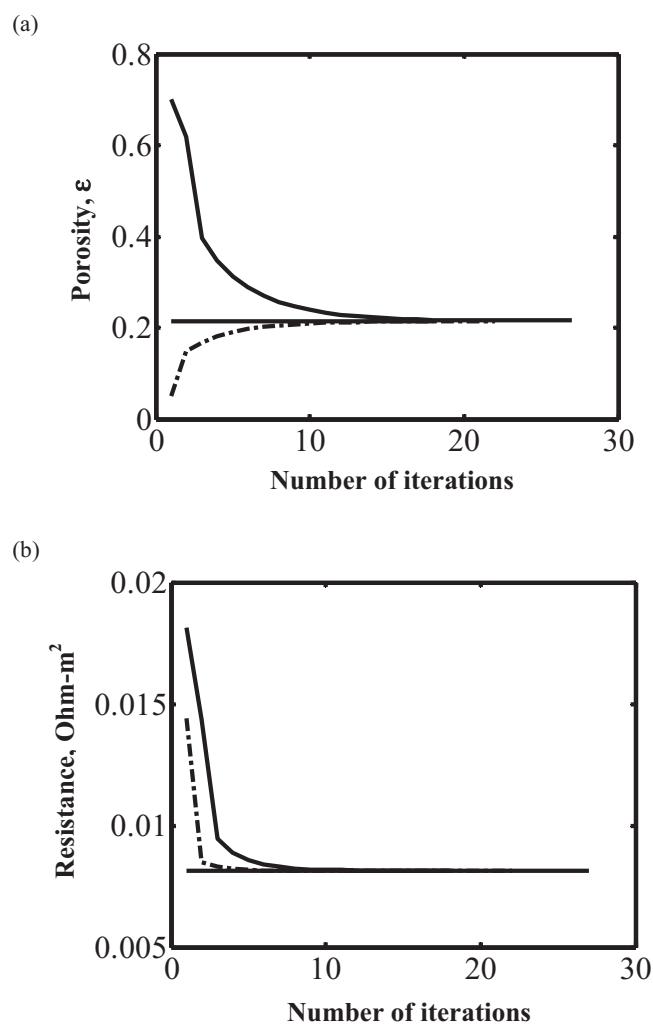
cate porous electrodes with smoothly varying porosity as a function of distance is difficult. A more practical way of representing graded porosity was applied here. The porosity profile was divided into N optimization zones, with constant porosity within each zone (see Fig. 3). For $N = 5$, the resistance across the electrode is minimized when the porosity is higher toward the electrode–separator interface (see Fig. 4) to have more electrolyte solution in the porous matrix. The optimal profile shows a significant decrease in pore volume at the other end, at the electrode–current collector interface. This optimization procedure shows improvement in electrode performance of 17.2% compared to the base-case spatially uniform porosity of 0.4. The spatially varying optimized electrode porosity has 4% better performance than the optimal spatially uniform porosity ($\varepsilon \sim 0.2$, see Fig. 1) for the same chemistry. Porous electrodes with more complicated chemistry models or different chemistry models, and optimization with additional physical constraints on the design, can have different performance improvements when using spatially varying porosity. Increasing the value of the number of zones N above 5, while being more difficult to fabricate, does not show much improvement in the performance. For instance, an improvement of 0.1% was obtained for $N = 12$ compared to $N = 5$. The choice of $N = 5$ provides a good trade-off between optimality and manufacturability.

Now consider the same optimal design problem but with the additional constraint of having a specified amount of active material
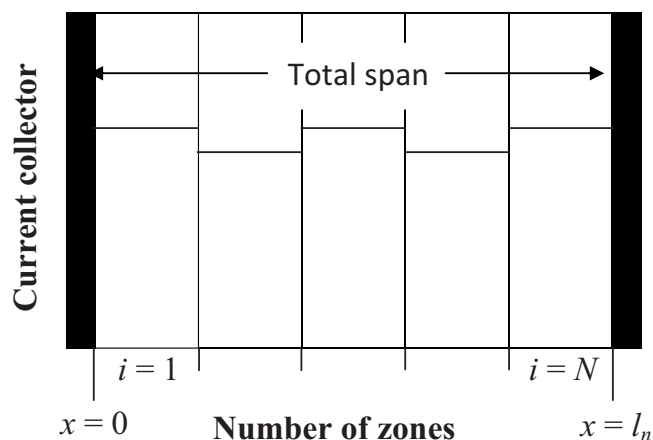
Figure 3. Schematic of an electrode of a lithium-ion battery divided into *N* optimization zones.

in the electrode, which is equivalent to having a fixed value for the porosity averaged across the electrode. For a fixed average porosity $\bar{\varepsilon} = 0.3$, the performance improvement is 15% compared to the base case, while having an optimal porosity profile that is qualitatively similar to that without the average porosity constraint (compare Fig. 4a and 5a). A qualitatively similar optimal porosity profile is obtained for a fixed average porosity $\bar{\varepsilon} = 0.5$ while providing a performance improvement of 33% over the base case.

Figure 6 shows the applied current profile across the electrode for the optimized and base-case design. The optimized current at the electrode–current collector interface is higher in magnitude due to lower resistance. The spatial variation in the electrolyte-phase potentials follows a similar qualitative trend but is very different quantitatively (see Fig. 7). The solid-phase potential in both cases does not show much variation across the electrode (see Fig. 8). The net potential drop $(\Phi_1 - \Phi_2)$ at the electrode–current collector interface is greater in the base case compared to the optimized case, indicative of the lower resistance inside the cell with optimized porosity profile.

Due to limited manufacturing precision and capacity fade, model parameters will vary somewhat from one electrode to the next. The importance of quantifying the effects of such uncertainties on the performance of nano- and microstructured materials is well established;[23] it has been shown for many materials systems that most to all of the benefits of optimization can be lost when uncer-
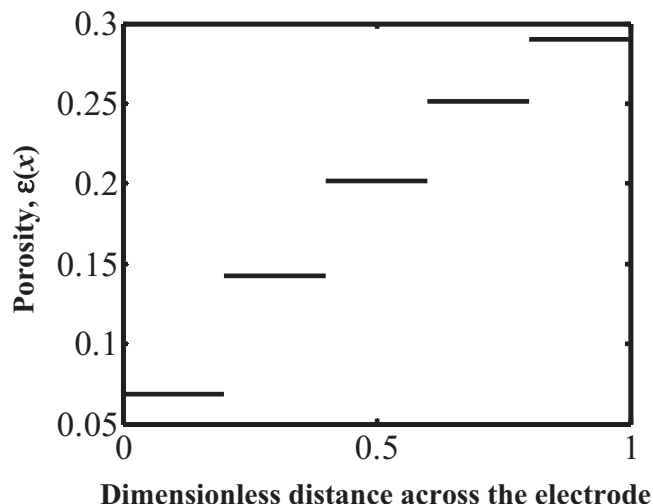

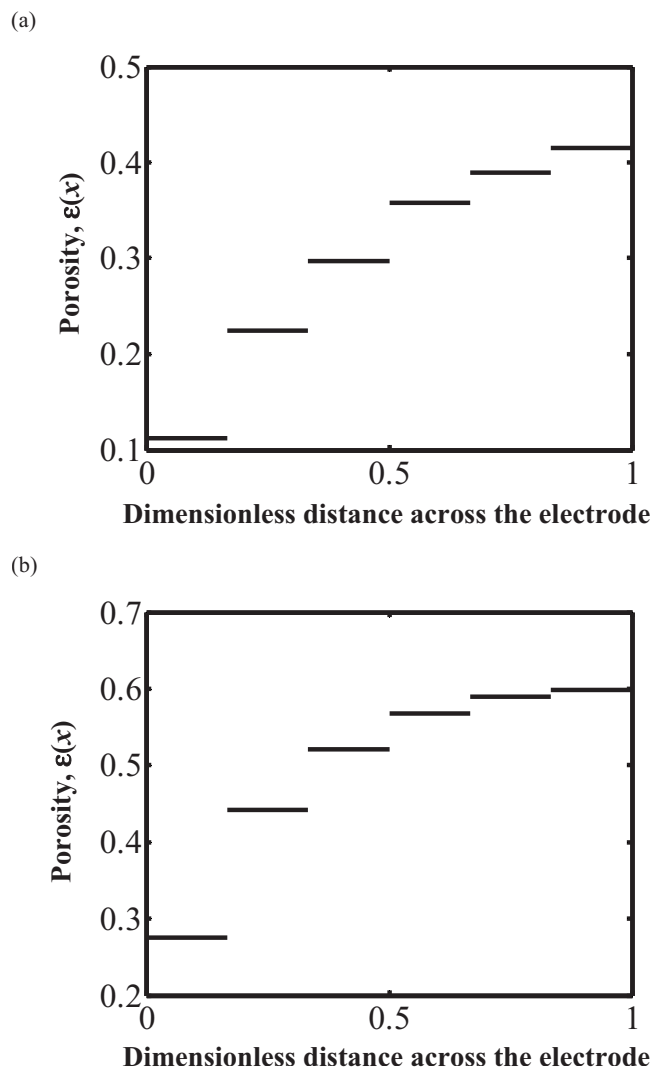**Figure 5.** Optimum porosity profile for $N = 6$ optimization zones for a fixed average porosity of (a) 0.3 and (b) 0.5.

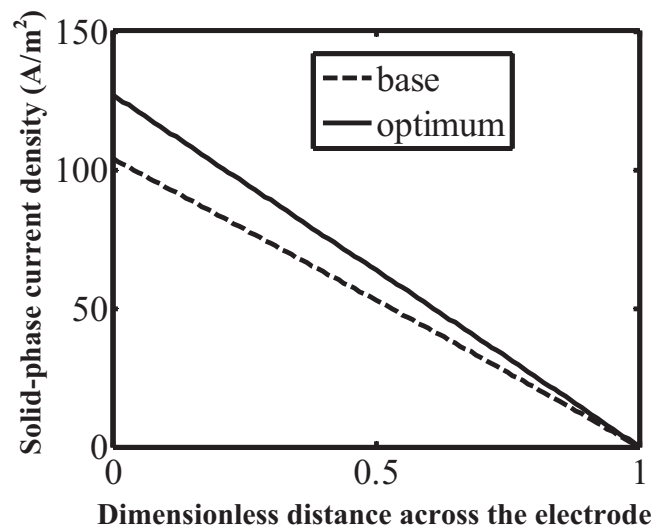**Figure 4.** Optimal porosity profile for $N = 5$ optimization zones.

Figure 6. Solid phase current profile across the electrode in base-case and optimized designs.
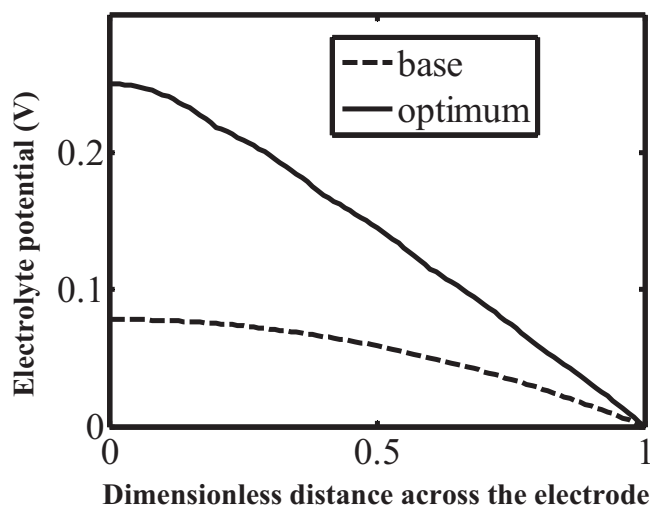
Figure 7. Electrolyte-phase potential profile in base-case and optimized designs.

Figure 9. Probability distribution function for the ohmic resistance for electrodes with spatially uniform porosities of $\varepsilon = 0.4$ (base) and obtained by optimization ($\varepsilon = 0.213\,88$).

tainties are ignored.[24,25] The uncertainties in the model parameters were described by Gaussian distributions with standard deviations that are 10% of the nominal parameter values. The probability distribution functions (pdfs) for the ohmic resistance for spatially uniform electrode porosities indicate that the optimized design is more robust to uncertainties in comparison to a nonoptimized porosity, with a reduction in variance for the optimal design of $\sim$40% (see Fig. 9). The design with the optimized spatially varying porosity is slightly more robust, with a reduction of variance of $\sim$43%, compared to a nonoptimized porosity (see Fig. 10). The robustness could be further enhanced by explicitly including uncertainty quantification into the optimization formulation.[26]

Conclusions

Model-based optimization was applied to the design of a spatially varying porosity profile in a next-generation porous electrode to minimize its ohmic resistance. The implementation of control vector parameterization is demonstrated for a simple porous electrode model. The parameters used for the electrode were based on the cobalt oxide chemistry, generally used in commercial lithium-ion batteries. The solid-phase intercalation phenomenon is not included in this work at this stage and is typically an important limiting factor for cobalt oxide and other intercalation electrodes. The
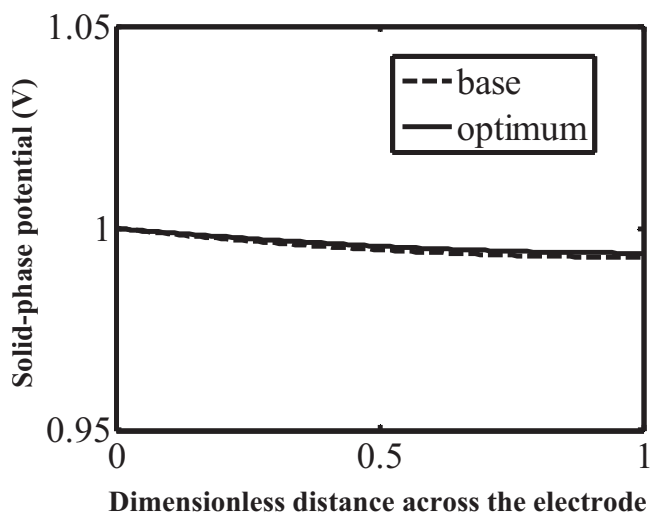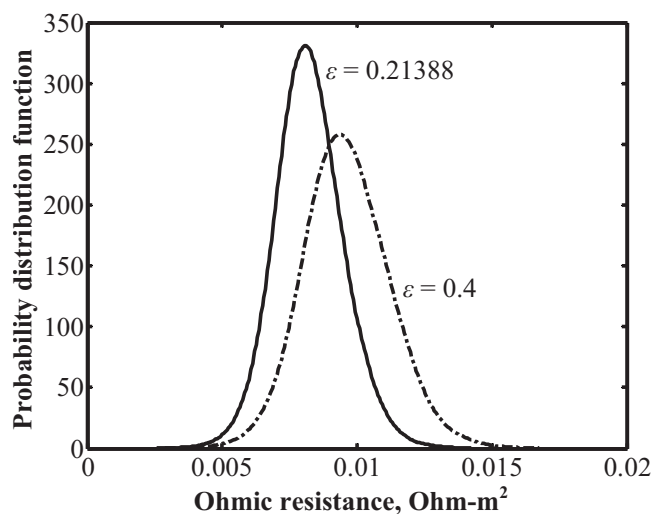
optimal design of graded porosity was found to reduce the ohmic resistance by 15%–33% without increasing the amount of active material. The optimal porosity grading was predicted to have 40% lower variation in the ohmic resistance to variations in model parameters due to manufacturing imprecision or capacity fade. The results suggest the potential for the simultaneous model-based design of electrode material properties that employ more detailed physics-based first-principles electrochemical engineering models to determine optimal design values to manufacture and evaluate experimentally. Further investigations into a whole-cell battery model may lead to engineering design alternatives that better satisfy energy and power requirements for emerging applications for batteries in vehicles, satellites, and in the military.

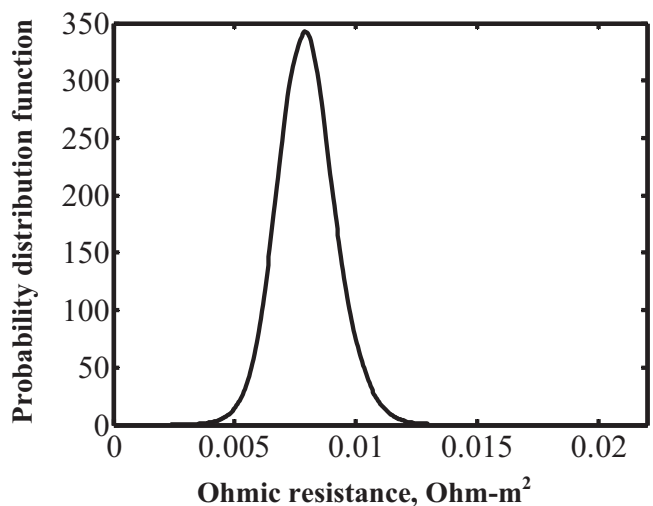**Figure 8.** Solid phase potential profile in base-case and optimized designs.

Figure 10. Probability distribution function for the ohmic resistance for an electrode with optimal spatially varying porosity.

Appendix

For a porous electrode with linear kinetics, Eq. 1-11 can be integrated analytically as

$$i_1 = a \cosh\left(\nu \frac{x}{l_p}\right) + b \sinh\left(\nu \frac{x}{l_p}\right) + \frac{\sigma i_{app}}{\sigma + \kappa}$$

$$\Phi_1 = a_1 \cosh\left(\nu \frac{x}{l_p}\right) + b_1 \sinh\left(\nu \frac{x}{l_p}\right) + c + \frac{i_{app} x}{\sigma + \kappa}$$

$$\Phi_2 = a_2 \cosh\left(\nu \frac{x}{l_p}\right) + b_2 \sinh\left(\nu \frac{x}{l_p}\right) + c + \frac{i_{app} x}{\sigma + \kappa} \qquad [A-1]$$

There are only three constants of integration (a,b,c). The coefficients a_1, b_1, a_2, b_2 depend on these three constants and other model parameters. With the boundary conditions, the resistance can be obtained as

$$Z = \frac{l_p\left(1 + \dfrac{2 + \left(\dfrac{\kappa}{\sigma} + \dfrac{\sigma}{\kappa}\right)\cosh(\nu)}{\nu \, \sinh(\nu)}\right)}{\kappa + \sigma} \qquad [A-2]$$

where $\nu = l_p \sqrt{(\kappa + \sigma)ai_0 F(\alpha_1 + \alpha_2)/\kappa\sigma RT}$.

This analytical solution has been previously used in the literature.[2] Similar equations for Φ_1, Φ_2, and i_2 can be obtained for any number of stages, but the constants are too messy to be reported here in closed form. The constants are found by matching the dependent variables at the interfaces. The numerical solution of the original BVPs is used for the results reported in the paper, as the constants for the analytical solutions cannot be conveniently used for optimization purposes. In addition, the results obtained for the numerical solution can be conveniently used for nonlinear kinetics as a starting point or initial guess.

References

1. M. Doyle, T. F. Fuller, and J. Newman, *J. Electrochem. Soc.*, **140**, 1526 (1993).
2. W. Tiedemann and J. Newman, *J. Electrochem. Soc.*, **122**, 1482 (1975).
3. T. F. Fuller, M. Doyle, and J. Newman, *J. Electrochem. Soc.*, **141**, 1 (1994).
4. T. F. Fuller, M. Doyle, and J. Newman, *J. Electrochem. Soc.*, **141**, 982 (1994).
5. M. Doyle and J. Newman, *J. Power Sources*, **54**, 46 (1995).
6. M. Doyle and J. Newman, *Electrochim. Acta*, **40**, 2191 (1995).
7. J. Newman, *J. Electrochem. Soc.*, **142**, 97 (1995).
8. V. Srinivasan and J. Newman, *J. Electrochem. Soc.*, **151**, A1530 (2004).
9. J. Christensen, V. Srinivasan, and J. Newman, *J. Electrochem. Soc.*, **153**, A560 (2006).
10. S. Stewart, P. Albertus, V. Srinivasan, I. Plitz, N. Pereira, G. Amatucci, and J. Newman, *J. Electrochem. Soc.*, **155**, A253 (2008).
11. V. R. Subramanian, V. Boovaragavan, and V. D. Diwakar, *Electrochem. Solid-State Lett.*, 255 (2007).
12. V. R. Subramanian, V. Boovaragavan, V. Ramadesigan, and M. Arabandi, *J. Electrochem. Soc.*, **156**, A260 (2009).
13. V. R. Subramanian, V. Boovaragavan, V. Ramadesigan, K. Chen, and R. D. Braatz, in *Design for Energy and the Environment: Proceedings of the Seventh International Conference on the Foundations of Computer-Aided Process Design*, M. M. El-Halwagi and A. A. Linninger, Editors, p. 987, CRC Press, Boca Raton (2009).
14. R. E. Garcia, Y. M. Chiang, W. C. Carter, P. Limthongkul, and C. M. Bishop, *J. Electrochem. Soc.*, **152**, A255 (2005).
15. G. Ceder, M. K. Aydinol, and A. F. Kohan, *Comput. Mater. Sci.*, **8**, 161 (1997).
16. N. Akaiwa, K. Thornton, and P. W. Voorhees, *J. Comput. Phys.*, **173**, 61 (2001).
17. Any maximization can be written as a minimization by multiplication of the objective by −1.
18. S. Kameswaran and L. T. Biegler, *Comput. Chem. Eng.*, **30**, 1560 (2006).
19. O. von Stryk and R. Bulirsch, *Ann. Operat. Res.*, **37**, 357 (1992).
20. M. Schlegel, K. Stockmann, T. Binder, and W. Marquardt, *Comput. Chem. Eng.*, **29**, 1731 (2005).
21. A. B. Singer and P. I. Barton, *J. Global Optim.*, **34**, 159 (2006).
22. D. W. Marquardt, *SIAM J. Appl. Math.*, **11**, 431 (1963).
23. R. D. Braatz, R. C. Alkire, E. Seebauer, E. Rusli, R. Gunawan, T. O. Drews, X. Li, and Y. He, *J. Process Control*, **16**, 193 (2006).
24. Z. K. Nagy and R. D. Braatz, *IEEE Trans. Control Syst. Technol.*, **11**, 494 (2003).
25. Z. K. Nagy and R. D. Braatz, *J. Process Control*, **17**, 229 (2007).
26. Z. K. Nagy and R. D. Braatz, *J. Process Control*, **14**, 411 (2004).